

Optical Engineering

OpticalEngineering.SPIEDigitalLibrary.org

Expanding the field-of-view and profile measurement of covered objects in continuous-wave terahertz reflective digital holography

Dayong Wang
Yanlin Zhao
Lu Rong
Min Wan
Xiaoyu Shi
Yunxin Wang
John T. Sheridan

SPIE.

Dayong Wang, Yanlin Zhao, Lu Rong, Min Wan, Xiaoyu Shi, Yunxin Wang, John T. Sheridan, "Expanding the field-of-view and profile measurement of covered objects in continuous-wave terahertz reflective digital holography," *Opt. Eng.* **58**(2), 023111 (2019), doi: 10.1117/1.OE.58.2.023111.

Expanding the field-of-view and profile measurement of covered objects in continuous-wave terahertz reflective digital holography

Dayong Wang,^{a,b} Yanlin Zhao,^a Lu Rong,^{a,b,*} Min Wan,^c Xiaoyu Shi,^a Yunxin Wang,^{a,b} and John T. Sheridan^c

^aBeijing University of Technology, College of Applied Sciences, Beijing, China

^bBeijing Engineering Research Center of Precision Measurement Technology and Instrument, Beijing, China

^cUniversity College Dublin, School of Electrical and Electronic Engineering, Dublin 4, Ireland

Abstract. Terahertz waves have unique propagation and penetration ability, and these reasons have been widely used in nondestructive testing. Compared with other terahertz imaging approaches, terahertz digital holography can retrieve both quantitative amplitude and phase information about an object wavefront in real time. A continuous-wave terahertz reflective digital holographic method is proposed for measuring the profile of covered objects. Subpixel image registration and image fusion algorithms are presented to expand the field-of-view (FOV) of the system. The validity of the proposed method is verified by the experiment using an optical pumped far-IR gas laser and a pyroelectric array detector. The profile of a metallic bookmark covered by a polytetrafluoroethylene plate is obtained. The FOV is expanded by a factor of 1.75 compared with that of a reconstruction performed employing single hologram. © 2019 Society of Photo-Optical Instrumentation Engineers (SPIE) [DOI: 10.1117/1.OE.58.2.023111]

Keywords: terahertz imaging; digital holography; nondestructive testing; digital imaging processing.

Paper 181558 received Oct. 30, 2018; accepted for publication Feb. 7, 2019; published online Feb. 23, 2019.

1 Introduction

The terahertz (THz) band lies between the microwave and the infrared regions. Frequencies range from 0.1 to 10 THz corresponding to wavelengths from 3 mm to 30 μm . The waves have unique propagation characteristics and can penetrate nonpolar materials, such as plastic, paper, and ceramics. Multiple THz nondestructive testing methods have been proposed and applied in biomedical imaging,^{1,2} security inspection,^{3,4} and material performance characterization.⁵ THz-pulsed imaging involves the generation and detection of THz femtosecond pulses, with object information retrieved by raster scanning and time-delay. However, using this method, it is difficult to retrieve full-field distribution in real time.^{6–8} Continuous-wave (CW) THz confocal scanning imaging maps the amplitude distribution point-by-point, the resolution of which depends on the illumination beam size.^{9,10} THz tomography obtains the three-dimensional absorption distribution of the object by reconstructing the projection map. The imaging speed is not fast and the resolution is limited.^{11,12}

THz digital holography records the interference pattern between the object beam and the reference beam and reconstructs the quantitative amplitude and phase distributions of the object wavefront through diffraction propagation.^{13–15} CW THz off-axis reflective digital holography can be used to measure the profile of reflective objects, including covered or coated ones, from the reconstructed phase distribution.^{16,17} Locatelli et al.¹⁸ proposed an off-axis reflective THz digital holographic approach obtaining the amplitude distribution of a metallic plate covered by a polypropylene mask coating, achieving a lateral resolution of 200 μm and a field-of-view (FOV) of 16 mm \times 12 mm. Hack and Zolliker¹⁹ obtained a

similar resolution (200 μm) and the same FOV employing a synthetic aperture and achieved a relative phase sensitivity about 6 μm . Topography measurement of the Siemens star covered by a Teflon plate was realized by recording three different interference patterns with an FOV of 8.16 mm \times 10.8 mm.²⁰ Although the covering mask would be penetrated by terahertz radiation, the former of which would still degrade the reconstruction quality of terahertz off-axis digital holography.^{18,20} In addition, it is very necessary to expand the FOV of off-axis holography beyond the restraint from the illumination spot size on the object plane.

In this paper, we proposed a modified method, based on CW THz reflective off-axis digital holography to measure the amplitude and profile distributions of a covered object, expanding the FOV using subpixel image registration and image fusion. A holographic system based on an optically pumped far-IR gas laser and a pyroelectric array detector was implemented. Applying this system, the profile of a metallic bookmark, covered by a polytetrafluoroethylene (PTFE) plate, is reported and performance discussed. The structure of this paper is as follows: Sec. 2 briefly describes the principle of off-axis digital holography, as well as the methods of subpixel image registration and image fusion. Section 3 describes the experimental setup and the reconstruction results. Finally, a summary concludes the paper.

2 Method

2.1 Off-Axis Digital Holography

We examine an off-axis digital holography system, the object plane is labeled (x_0, y_0) and the recording plane is (x, y) . A beam of wavelength λ is divided by a beam splitter into two parts, the wavefront of one part is modulated by the object

*Address all correspondence to Lu Rong, E-mail: ronglu@bjut.edu.cn

producing the object beam, and the other part propagates to the recording plane at a known fixed angle to the object beam, as this is the reference beam. The object beam and the reference beam in recording plane are denoted by $O(x, y)$ and $R(x, y)$, respectively. The complex amplitude distribution $U(x, y)$ and the intensity of the hologram $I(x, y)$ in the recording plane can be related as follows:

$$I(x, y) = |U(x, y)|^2 = |O(x, y) + R(x, y)|^2. \quad (1)$$

Fourier spectrum filtering is performed to filter out the zero-order and -1 order in the frequency domain, and the filtered hologram $I_f(x, y)$ is obtained by inverse Fourier transforming the $+1$ -order part of the spectrum. The complex amplitude distribution of the object wavefront in the object plane is obtained numerically using the angular spectrum algorithm to simulate propagation wave²¹

$$O'(x_0, y_0) = \text{IFFT}\{\text{FFT}[I_f(x, y)]H(f_x, f_y)\}, \quad (2)$$

where FFT and IFFT are Fourier transform and inverse Fourier transform, respectively, f_x and f_y are the spatial frequency domain coordinates, $H(f_x, f_y)$ denotes the optical transfer function of free space

$$H(f_x, f_y) = \exp\left[\frac{-j2\pi z}{\lambda} \sqrt{1 - (\lambda f_x)^2 - (\lambda f_y)^2}\right], \quad (3)$$

where z is the propagation distance from the recording plane to the object plane. The reconstructed amplitude distribution of the object $o'(x_0, y_0)$ is the absolute value of the $O'(x_0, y_0)$. The reconstructed phase distribution of the object is

$$\varphi'(x_0, y_0) = \arctan\left\{\frac{\text{Im}[O'(x_0, y_0)]}{\text{Re}[O'(x_0, y_0)]}\right\} \quad \varphi' \in [-\pi, \pi). \quad (4)$$

The phase distribution calculated by inverse tangent function in Eq. (4) is phase wrapped, and the phase takes values between $-\pi$ and π (modulo π). The phase distribution obtained by digital holography can be used to extract the profile of the reflective object after phase aberration correction and phase unwrapping. For reflective object (in air $n = 1$), the profile height distribution $h(x_0, y_0)$ is

$$h(x_0, y_0) = \frac{\varphi'(x_0, y_0)\lambda}{4\pi n}. \quad (5)$$

2.2 Subpixel Image Registration and Image Fusion

Assuming that the detector has $M \times N$ pixels with a rectangular pixel size of Δr , the FOV of the system is $L_x = M\Delta r$ and $L_y = N\Delta r$. The methods of expanding the FOV in visible light digital holography include preimaging^{22,23} and image fusion.²⁴ The former places an imaging lens in front of the detector, and the focal plane of the detector serves as the virtual recording hologram. The FOV of which is determined by the values of the cross-sectional beam size and the magnification of the imaging systems. In the case of THz imaging, the imaging setup should ideally be compact and lensless to maintain reasonable resolution and signal-to-noise ratio. The latter records the holograms of the different

regions of the object then fuses multiple holograms or multiple reconstructed images to expand the FOV of system.

In this paper, a number of holograms were recorded follow shifts of the object horizontally. An image fusion approach to reconstruct the wavefront is proposed. The method consists of three steps: image registration, weighted smoothing, and image fusion.

First, the relative displacement of the reconstructed images is accurately determined by image registration. Assuming the reconstructed amplitude images of neighborhood region i and region $i + 1$ are $o'_i(x_0, y_0)$ and $o'_{i+1}(x_0, y_0)$, respectively. Overlapping subsections are designated two new images $s_i(x_0, y_0)$ and $s_{i+1}(x_0, y_0)$, respectively, having the same size $\xi \times \eta$. The relative displacement of the images is calculated using nonlinear optimization and discrete Fourier transform to within a small fraction of a pixel.²⁵ The image $s_{i+1}(x_0, y_0)$ is considered has a global coordinate translation $(\Delta x, \Delta y)$ to the image $s_i(x_0, y_0)$, to within multiplication by an arbitrary constant α . A standard FFT-based numerical approach is applied to find the cross correlation peak within a pixel

$$\begin{aligned} r_{s_i s_{i+1}}(\Delta x, \Delta y) &= \sum_{x_0, y_0} s_i(x_0, y_0) s_{i+1}^*(x_0 - \Delta x, y_0 - \Delta y), \\ &= \sum_{f_x, f_y} S_i(f_x, f_y) S_{i+1}^*(f_x, f_y) \\ &\quad \times \exp\left[i2\pi\left(\frac{f_x \Delta x}{\xi} + \frac{f_y \Delta y}{\eta}\right)\right], \end{aligned} \quad (6)$$

where $r_{s_i s_{i+1}}$ is the cross correlation of $s_i(x_0, y_0)$ and $s_{i+1}(x_0, y_0)$, “*” denotes complex conjugation, $S_i(f_x, f_y)$ and $S_{i+1}(f_x, f_y)$ are the discrete Fourier transforms of $s_i(x_0, y_0)$ and $s_{i+1}(x_0, y_0)$

$$S_i(f_x, f_y) = \sum_{x_0, y_0} \frac{s_i(x_0, y_0)}{\sqrt{\xi\eta}} \exp\left[-i2\pi\left(\frac{f_x x_0}{\xi} + \frac{f_y y_0}{\eta}\right)\right]. \quad (7)$$

The normalized root-mean-square (RMS) error metric E is used to quantify the error between $s_i(x_0, y_0)$ and $s_{i+1}(x_0, y_0)$

$$\begin{aligned} E^2 &= \min_{\alpha, \Delta x, \Delta y} \frac{\sum_{x_0, y_0} |\alpha s_i(x_0 - \Delta x, y_0 - \Delta y) - s_{i+1}(x_0, y_0)|^2}{\sum_{x_0, y_0} |s_i(x_0, y_0)|^2}, \\ &= 1 - \frac{\max_{\Delta x, \Delta y} |r_{s_i s_{i+1}}(\Delta x, \Delta y)|^2}{\sum_{x_0, y_0} |s_i(x_0, y_0)|^2 \sum_{x_0, y_0} |s_{i+1}(x_0, y_0)|^2}. \end{aligned} \quad (8)$$

The smaller the RMS error E , the greater the image similarity, the closer the alignment. A matrix multiplication implementation of the two-dimensional discrete Fourier transform is used to refine the initial peak location estimate. Subpixel registration is achieved by searching the cross correlation peak in a 1.5×1.5 pixel neighborhood (in units of the original pixel). The relative displacement between the reconstructed images $(\Delta M, \Delta N)$ can be obtained in this way using the overlap sections.

Then, weighted smoothing is used to reduce the amplitude difference and phase shift caused by any nonuniformity in the uneven distribution of THz beams in the experimental

setup. For the reconstructed amplitude images, with overlap sections as the reference, a suitable normalization factor of $o'_{i+1}(x_0, y_0)$ is given as

$$r_o = \frac{\sum_{\Delta M, \Delta N}^{M, N} o'_i / \sum_{1,1}^{M-\Delta M+1, N-\Delta N+1} o'_{i+1}}{\quad} \quad (9)$$

The normalized amplitude distribution of $o'_{i+1}(x_0, y_0)$ is then

$$o''_{i+1}(x_0, y_0) = o'_{i+1}(x_0, y_0) r_o. \quad (10)$$

For the reconstructed phase images, with overlap sections as the reference, the resulting corrected phase shift of $\varphi'_{i+1}(x_0, y_0)$ is given as

$$r_\varphi = \left(\sum_{\Delta M, \Delta N}^{M, N} \varphi'_i - \sum_{1,1}^{M-\Delta M+1, N-\Delta N+1} \varphi'_{i+1} \right) / (M - \Delta M) \times (N - \Delta N). \quad (11)$$

The corresponding normalized phase distribution of $\varphi'_{i+1}(x_0, y_0)$ is given as

$$\varphi''_{i+1}(x_0, y_0) = \varphi'_{i+1}(x_0, y_0) + r_\varphi. \quad (12)$$

Finally, bicubic interpolation²⁶ is applied to the resulting reconstructed images with an upsampling factor of 10, to provide accurate 0.1 pixel spaced sample values. The reconstructed images are expanded in size by zero padding, and image translation with the corresponding displacements is applied to the reconstructed images. Finally, the FOV of the system is successfully expanded by fusing the multiple reconstructed amplitude and phase images.

3 Experiments and Results

3.1 Experimental Setup

An experimental setup for CW THz reflective off-axis digital holography for covered object profile measurement was shown in Fig. 1(a). The THz source was an optical pumped far-IR gas laser (FIRL 295, Edinburgh Instrument). Its central wavelength is 118.83 μm (2.52 THz), and the maximum power is 500 mW. Two off-axis parabolic mirrors (PM) were

used to collimate and expand the terahertz beam. The distribution of the collimated beam was recorded by the pyroelectric detector. And the diameter (full-width at half-maximum) was about 15.4 mm measured by cross-section intensity distribution. The collimated THz wave was divided into two beams by the HRFZ-Si beam splitter, whose splitting ratio at 2.52 THz is 54% for transmission and 46% for reflection. One beam propagated to the recording plane (reference beam) while the other beam illuminates the object producing the object beam. The interference angle was chosen ~ 0.61 rad, and the holograms were recorded by a pyroelectric array detector (Pyrocam IV, Ophir Spiricon), which has 320×320 pixels on an $80\text{-}\mu\text{m}$ pixel pitch.

The object is a metallic bookmark produced by photo etching [Fig. 1(b)]. It was placed at a distance of 63.0 mm upstream from the detector to ensure adequate resolution. The object plane and the recording plane are not parallel as shown in Fig. 1. In order to verify the imaging capability of the system for covered objects, a 1.5-mm-thick PTFE plate ($n = 1.43$) was placed in front of the bookmark [Fig. 1(c)]. This plate can be seen to opaque in the visible band, and the surface of the covered plate is not completely homogeneous due to machining error. The object was placed on a manual linear stage capable of applying up to 25.4 mm of smooth motion, and different regions of the object were illuminated by moving the object.

3.2 Reconstructed Results of the Single Hologram

The reconstructed results of the metallic bookmark with and without the PTFE plate present were compared. It was found that the preprocessing of 100 frames is required to improve the fringe contrast of the holograms. The holograms for the same region of the object without and with PTFE plate are shown in Figs. 2(a1) and 2(a2). The period of the resulting interference fringe is 4.81 lp/mm. As can be seen, the contrast of the hologram is degraded when the PTFE plate is presented because of the inhomogeneity of the covered mask. An autofocus algorithm²⁷ was applied to determine the reconstructed distance. The distance was 63.0 mm in the uncovered case and 63.65 mm in the covered case because of the optical path difference caused by the different refractive index of the air and PTFE. The theoretical lateral resolution of the imaging system is $\delta = \lambda d / N \Delta r = 292.4 \mu\text{m}$. An angular spectrum algorithm was used to obtain the amplitude

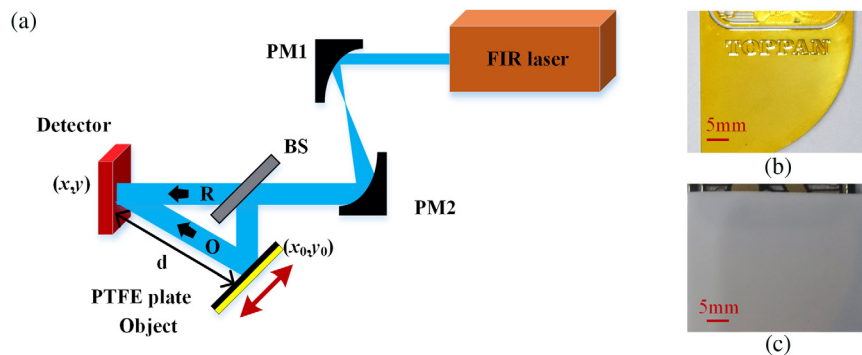


Fig. 1 (a) CW THz reflective off-axis digital holography experimental setup for covered object measurement, PMs represent off-axis parabolic mirrors, the focal length of PM1 and PM2 are 50.8 and 101.6 mm, respectively, BS is a THz beam splitter. The distance from the object plane to the recording plane is d . (b) Photo of the imaged metallic bookmark. (c) The same metallic bookmark covered by a 1.5-mm plate.

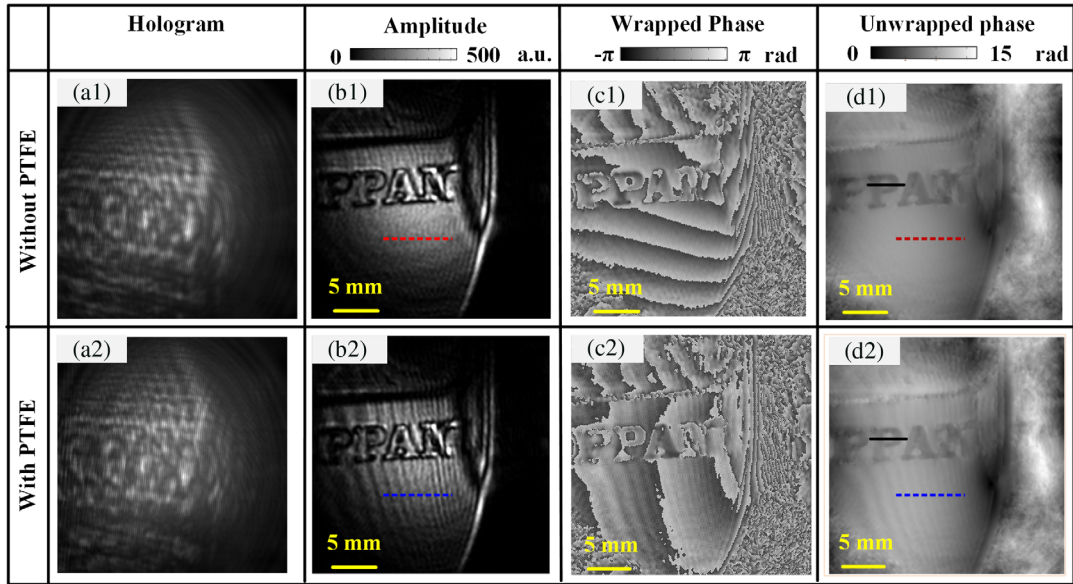


Fig. 2 The reconstructed results of single region. (a1) and (a2) Holograms without and with PTFE plate. (b1–d1) Reconstructed amplitude, wrapped phase, and unwrapped phase without PTFE plate. (b2–d2) Reconstructed amplitude, wrapped phase, and unwrapped phase with PTFE plate.

and wrapped phase distributions of the object. The reconstructed amplitude distributions are shown in Figs. 2(b1) and 2(b2), the etched letters can be visually distinguished. It is noted that significant noise is introduced by the inclined plane (the object plane is nonparallel to the recorded plane) and surface roughness of the PTFE plate. The wrapped phase distributions of the object are shown in Figs. 2(c1) and 2(c2). A least square phase unwrapping algorithm²⁸ was used to obtain the continuous phase distributions. With regarded to the phase aberration caused by the intersection angle between object plane and recording plane, the one-step-method²⁹ was applied. The unwrapped phases are shown in Figs. 2(d1) and 2(d2). As can be seen, diffraction at the curve edge of the bookmark reduces the reconstruction quality of the adjacent area.

In order to show the influence of the PTFE plate on the reconstructed images, we compared the flat regions of the sample without alphabets. Figure 3 shows the amplitude and phase distribution curves taken along the dotted lines shown in Fig. 2. It can be seen that the variation of reconstructed images with the PTFE plate is large than those without the PTFE plate.

The profile of the object can be obtained from the unwrapped phase image as indicated in Sec. 2.1. In order to verify the measurement accuracy of the proposed method, cross-sectional profiles are taken along the lines shown in Figs. 2(d1) and 2(d2), the resulting profiles are plotted in Figs. 4(a) and 4(b) for reconstructions with and without the PTFE plate. The object was also directly measured by a three-dimensional (3-D) Surface Profiler (WYKO NT1100, Veeco) giving a depth result of $157.0 \mu\text{m}$. The profiles information only can be measured in integral pixels from the phase images. Choosing the same region for comparison, the calculated etching depths of the letter “P” were 161.6 and $150.6 \mu\text{m}$ in the uncovered case, and 166.4 and $163.9 \mu\text{m}$ in the covered case [see Figs. 4(a) and 4(b)]. The estimated etching depths of the letters are different on the left and right sides because of the phase distortion caused by the non-parallelism between the object plane and the recording plane. The experimental results indicate that the relative error of measuring the profiles of the object by CW THz digital holography are 2.93% and 4.08% in the uncovered case. The relative errors are 5.98% and 4.39% in the covered case, respectively. The accuracy of profiles measurement

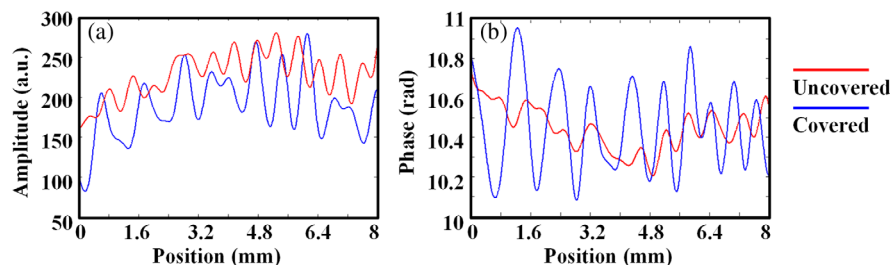


Fig. 3 The comparison curves of (a) the reconstructed amplitude and (b) phase distributions in Fig. 2. The red curves in Figs. 3(a) and 3(b) represent the red dotted lines in Figs. 2(b1) and 2(d1), respectively. The blue curves in Figs. 3(a) and 3(b) represent the blue dotted lines in Figs. 2(b2) and 2(d2), respectively.

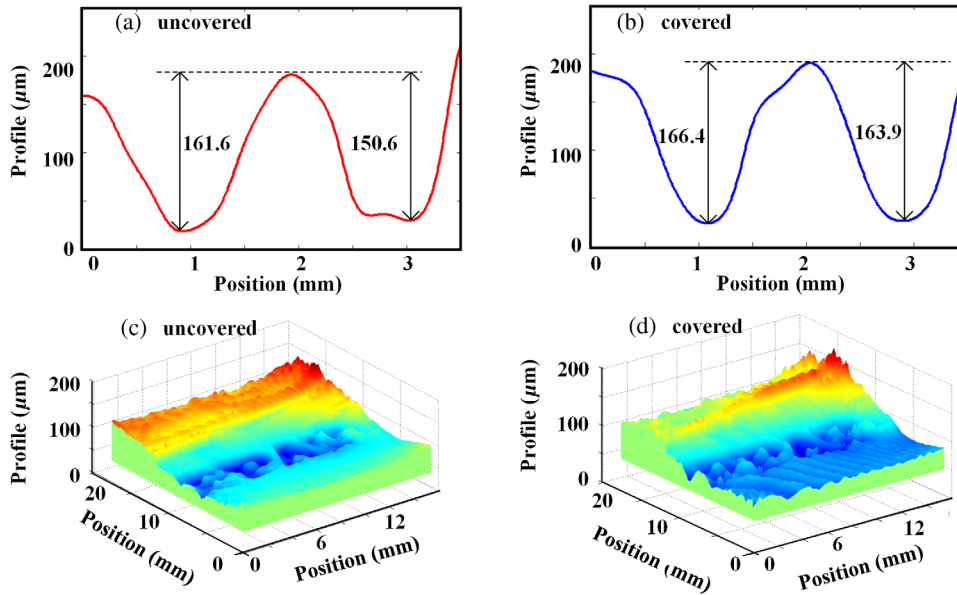


Fig. 4 (a), (b) Profiles of the object. The red curve and the blue curve represent the experimental data along the cross-sections highlighted in Figs. 2(d1) and 2(d2). (c) 3-D structure of the object without covered. (d) 3-D structure of the covered object.

needs to be further improved. In Figs. 4(c) and 4(d), the 3-D profiles of the bookmark are presented. From the 3-D maps, it can be seen that the upper part and the lower part are not in the same plane, which is consisted with the orientation the system. Moreover, for the flat regions without alphabets, we can see that the surface is undulate when the sample is covered. The experimental results clearly demonstrate that the THz system has the ability to detect the objects behind visually opaque materials such as PTFE.

3.3 Expanding the Field-of-View by Image Fusion

The width of the metallic bookmark used in the experiment is 34 mm. The illuminating beam size is less than the numerical aperture of the detector because of the limit aperture of beam splitter; therefore, the effective FOV of a single hologram captured using the system is about 320×250 pixels (25.6×20 mm²). In order to inspect the complete object, three holograms containing images of different regions of the object were recorded. The experiment was performed so that

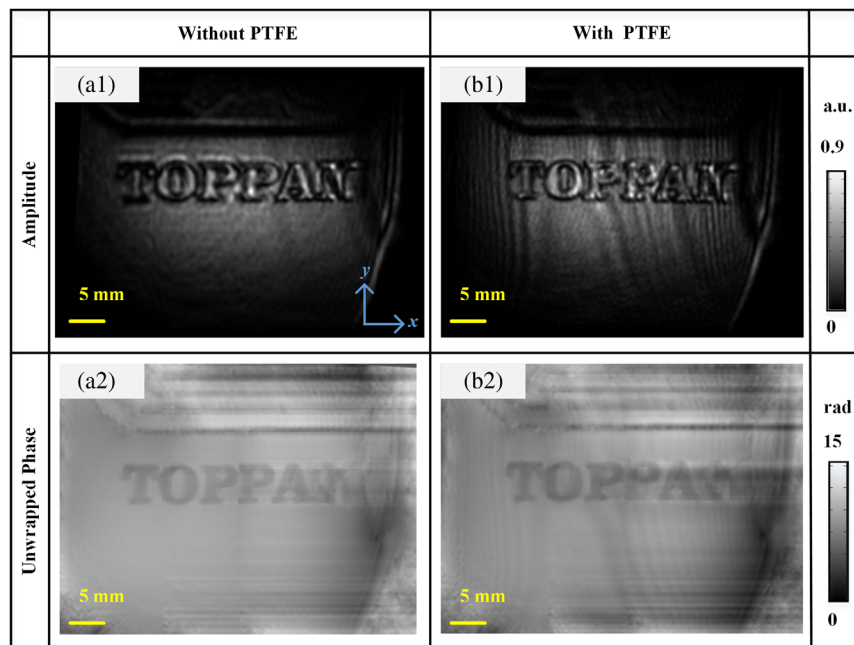


Fig. 5 The experimental results of expanding the FOV by subpixel image registration and image fusion. (a1), (b1) Reconstructed amplitude and phase of expanding the FOV. The bookmark was not covered. (a2), (b2) Reconstructed amplitude and phase after expanding the FOV. The bookmark was covered behind a 1.5-mm-thick PTFE plate.

images with overlap parts appeared in the adjacent holograms. The reconstructed images were fused by the method proposed in Sec. 2.2. The lateral and longitudinal relative displacement between region 2 and region 1 are 83.2 and -4.6 pixels, respectively. The lateral and longitudinal relative displacement between region 3 and region 2 are 82.8 and -6.5 pixels, respectively. The amplitude and phase distribution of the object after image fusion are shown in Figs. 5(a1) and 5(b1), when the bookmark was not covered. After being covered by the PTFE plate, the amplitude and phase distribution of the bookmark are shown in Figs. 5(a2) and 5(b2). With our proposed method, the FOV of the system is expanded to $25.6 \times 35 \text{ mm}^2$, a factor of 1.75 times larger than the initial single hologram value. The intensity of the illuminating THz field is uneven, so the image quality of the reconstructed image after image fusion is degraded.

4 Conclusions

In this paper, we proposed a CW THz reflective digital holography approach for covered object profile measurement. Subpixel image registration and image fusion algorithms were used to expand the FOV. The experimental results demonstrate that the proposed method can successfully obtain the amplitude and phase distributions of the object covered by the opaque material. Compared to the measurements performed using a commercial 3-D Surface Profiler, the etch depths of object were determined to a relative error of 2.93%, 4.08%, 5.98%, and 4.39%, respectively. The FOV of the system is improved by a factor of 1.75. The FOV is only limited by the size of the object imaged and can be further expanded. It is noted that the major error comes from roughness and uneven surfaces of the covered plate, which would increase speckle noise in the reconstructed images and inaccuracy of etching depth in the reconstructed phase distributions. Another minor negative factor comes from intensity instability of the illuminating THz beam. This issue can be alleviated using the proposed weighted smoothing algorithm in Eqs. (9)–(12). CW THz reflective digital holography is therefore shown to have potential for covered object profile measurement. It is intended to further improve resolution, reduce measurement error, and apply the proposed method to larger objects in the future.

Acknowledgments

This work was financially supported by the National Natural Science Foundation of China (61675010, 61475011) and Science Foundation of Education Commission of Beijing (KZ201610005008), Beijing Nova Program (XX2018072). M. W. acknowledges the financial supports by CELTA (675683) in the Horizon 2020 program.

References

- L. Rong et al., "Terahertz in-line digital holography of human hepatocellular carcinoma tissue," *Sci. Rep.* **5**, 8445 (2015).
- L. Guo et al., "Observation of dehydration dynamics in biological tissues with terahertz digital holography," *Appl. Opt.* **56**(13), F173–F178 (2017).
- M. C. Kemp et al., "Security applications of terahertz technology," *Proc. SPIE* **5070**, 44–52 (2003).
- C. A. Martin et al., "High-resolution passive millimeter-wave security screening using few amplifiers," *Proc. SPIE* **6548**, 654806 (2007).
- W. Xiong and J. Shen, "Fingerprint extraction from interference destruction terahertz spectrum," *Opt. Express* **18**(21), 21798–21803 (2010).
- H. Lin et al., "Measurement of the intertablet coating uniformity of a pharmaceutical pan coating process with combined terahertz and optical coherence tomography in-line sensing," *J. Pharm. Sci.* **106**(4), 1075–1084 (2016).
- Z. D. Taylor et al., "Reflective terahertz imaging of porcine skin burns," *Opt. Lett.* **33**(11), 1258–1260 (2008).
- V. P. Wallace et al., "Three-dimensional imaging of optically opaque materials using nonionizing terahertz radiation," *J. Opt. Soc. Am. A* **25**(12), 3120–3132 (2008).
- Y. Zhou and Q. Li, "Dual-axis reflective continuous-wave terahertz confocal scanning polarization imaging and image fusion," *Opt. Eng.* **56**(1), 013103 (2017).
- Q. Song, Y. Zhao, and A. Redo, "Fast continuous terahertz wave imaging system for security," *Opt. Commun.* **282**(10), 2019–2022 (2009).
- B. Li et al., "Application of continuous-wave terahertz computed tomography for the analysis of chicken bone structure," *Opt. Eng.* **57**(2), 023105 (2018).
- B. Recur et al., "Investigation on reconstruction methods applied to 3D terahertz computed tomography," *Opt. Express* **19**(6), 5105–5117 (2011).
- N. V. Petrov et al., "Application of terahertz pulse time-domain holography for phase imaging," *IEEE Trans. Terahertz Sci. Technol.* **6**(3), 464–472 (2016).
- M. S. Heimbeck et al., "Terahertz digital holography using angular spectrum and dual wavelength reconstruction methods," *Opt. Express* **19**(10), 9192–9200 (2011).
- H. Huang et al., "Synthetic aperture in terahertz in-line digital holography for resolution enhancement," *Appl. Opt.* **55**(3), A43–A48 (2016).
- L. Hou et al., "Terahertz real-time off-axis digital holography with zoom function," *Chin. Phys. Lett.* **34**(5), 054207 (2017).
- D. G. A. Ibrahim, "Steep large film thickness measurement with off-axis terahertz digital holography reconstructed by a direct Fourier and Hermite polynomial," *Appl. Opt.* **57**(10), 2533–2538 (2018).
- M. Locatelli et al., "Real-time terahertz digital holography with a quantum cascade laser," *Sci. Rep.* **5**, 13566 (2015).
- E. Hack and P. Zolliker, "THz holography in reflection using a high resolution microbolometer array," *Opt. Express* **23**(9), 10957–10967 (2015).
- L. Valzania, P. Zolliker, and E. Hack, "Topography of hidden objects using THz digital holography with multi-beam interferences," *Opt. Express* **25**(10), 11038–11047 (2017).
- J. W. Goodman, *Introduction to Fourier Optics*, 3rd ed., Roberts & Company Englewood, Greenwood Village, Colorado, (2005).
- Y. Wu et al., "Coal powder measurement by digital holography with expanded measurement area," *Appl. Opt.* **50**(34), H22–H29 (2011).
- S. Liu et al., "Computer-generated hologram generation method to expand the field of view of the reconstructed image," *Appl. Opt.* **57**(1), A86–A90 (2018).
- V. Micó, C. Ferreira, and J. García, "Surpassing digital holography limits by lensless object scanning holography," *Opt. Express* **20**(9), 9382–9395 (2012).
- M. Guizar-Sicairos, S. T. Thurman, and J. R. Fienup, "Efficient subpixel image registration algorithms," *Opt. Lett.* **33**(2), 156–158 (2008).
- F. N. Fritsch and R. E. Carlson, "Monotone piecewise cubic interpolation: algorithms and software," *SIAM J. Numer. Anal.* **17**(2), 238–246 (1980).
- H. Huang et al., "Application of autofocusing methods in continuous-wave terahertz in-line digital holography," *Opt. Commun.* **346**, 93–98 (2015).
- M. D. Pritt and J. S. Shipman, "Least-squares two-dimensional phase unwrapping using FFT's," *IEEE Trans. Geosci. Remote Sens.* **32**(3), 706–708 (1994).
- O. Rincon, R. Amezquita, and F. Monroy, "Phase alteration compensation in reflection digital holography," *J. Phys.: Conf. Series* **274**, 12055 (2011).

Dayong Wang received his PhD from Xi'an Institute of Optics and Fine Mechanics, Chinese Academy of Sciences, in 1994. He joined Beijing University of Technology (BJUT) in 1996 and has been a professor since 2000. He was a postdoc in Weizmann Institute of Science, Israel, from 1998 to 2000, and a visiting professor in the Universität Stuttgart from 2006 to 2007. His research interests include optical information processing, terahertz imaging, and microwave photonics.

Yanlin Zhao received her BE degree in physics from Shanxi Normal University, China, in 2016. Currently, she is an MS degree candidate in physics at BJUT China. Her main research direction is terahertz digital holography.

Lu Rong received his BE and PhD degrees in Beihang University, China, in 2006 and 2012, respectively. He is currently an associate professor of optical engineering at College of Applied Sciences, BJUT. His research interests include terahertz imaging, phase, and tomographic microscopy.

Min Wan received her BE degree from Xi'an Technological University, China, in 2014, and her ME degree from BJUT, China, in 2017. She is a Marie Curie Early Stage Researcher and PhD candidate at the University College Dublin (UCD), Ireland. Her research interests are terahertz imaging, three-dimensional integral imaging, and holography.

Xiaoyu Shi received her BE degree from Tianjin University of Technology and Education, China, in 2012, and received her PhD from Beijing Normal University, China, in 2018. She is a postdoc in BJUT. Her research interests include random laser, advanced optical material, and terahertz imaging.

Yunxin Wang received her MS and PhD degrees from Tianjin University in 2006 and 2009, respectively. Since then, she has

been employed at BJUT and became an associate professor in 2014. Her research interests include microwave photonics and digital holographic microscopy.

John T. Sheridan received his BE degree from the National University of Ireland, Galway, MScEE degree from Georgia Tech, and DPhil degree from Oxford University. He held an Alexander von Humboldt fellowship in Erlangen-Nürnberg. He is currently a professor of optical engineering at the School of Electrical and Electronic Engineering, UCD. He is the cofounder of Equilume Ltd., a fellow of SPIE and OSA, and coeditor of linear canonical transforms in the Springer Series in Optical Sciences.